Analytical incorporation of fractionation effects in probabilistic treatment planning for intensity-modulated proton therapy

Niklas Wahl,[1,2,3] Philipp Hennig,[4] Hans-Peter Wieser,[1,2,5] and Mark Bangert[a)1,2]

[1)] *Department of Medical Physics in Radiation Oncology, German Cancer Research Center - DKFZ, Im Neuenheimer Feld 280, D-69120 Heidelberg, Germany*

[2)] *Heidelberg Institute for Radiation Oncology - HIRO, Im Neuenheimer Feld 280, D-69120 Heidelberg, Germany*

[3)] *Fakultät für Physik und Astronomie, Universität Heidelberg, Im Neuenheimer Feld 226, D-69120 Heidelberg, Germany*

[4)] *Max-Planck Institute for Intelligent Systems, Spemannstraße 34, 72076 Tübingen, Germany*

[5)] *Medizinische Fakultät Heidelberg, Universität Heidelberg, Im Neuenheimer Feld 672, D-69120 Heidelberg, Germany*

(Dated: 12 February 2018)

[a)] Corresponding Author: m.bangert@dkfz.de

PURPOSE: We show that it is possible to explicitly incorporate fractionation effects into closed-form probabilistic treatment plan analysis and optimization for intensity-modulated proton therapy with analytical probabilistic modeling (APM). We study the impact of different fractionation schemes on the dosimetric uncertainty induced by random and systematic sources of range and setup uncertainty for treatment plans that were optimized with and without consideration of the number of treatment fractions.

METHODS: The APM framework is capable of handling arbitrarily correlated uncertainty models including systematic and random errors in the context of fractionation. On this basis, we construct an analytical dose variance computation pipeline that explicitly considers the number of treatment fractions for uncertainty quantification and minimization during treatment planning. We evaluate the variance computation model in comparison to random sampling of 100 treatments for conventional and probabilistic treatment plans under different fractionation schemes (1, 5, 30 fractions) for an intracranial, a paraspinal and a prostate case. The impact of neglecting the fractionation scheme during treatment planning is investigated by applying treatment plans that were generated with probabilistic optimization for 1 fraction in a higher number of fractions and comparing them to the probabilistic plans optimized under explicit consideration of the number of fractions.

RESULTS: APM enables the construction of an analytical variance computation model for dose uncertainty considering fractionation at negligible computational overhead. It is computationally feasible (1) to simultaneously perform a robustness analysis for all possible fraction numbers and (2) to perform a probabilistic treatment plan optimization for a specific fraction number. The incorporation of fractionation assumptions for robustness analysis exposes a dose to uncertainty trade-off, i.e. the dose in the organs at risk is increased for a reduced fraction number and/or for more robust treatment plans. By explicit consideration of fractionation effects during planning, we demonstrate that it is possible to exploit this trade-off during optimization. APM optimization considering the fraction number reduced the dose in organs at risk compared to conventional probabilistic optimization neglecting the fraction number.

CONCLUSION: APM enables computationally efficient incorporation of fractionation effects in probabilistic uncertainty analysis and probabilistic treatment plan

optimization. The consideration of the fractionation scheme in probabilistic treatment planning reveals the trade-off between number of fractions, nominal dose, and treatment plan robustness.

PACS numbers: 87.55.de, 87.55.Gh, 87.55.kd
Keywords: random and systematic errors, uncertainty, inverse planning, proton therapy, fractionation

I. INTRODUCTION

In radiation therapy, the planned dose distributions is usually delivered through several treatment fractions. The fractionation scheme is chosen mainly under consideration of biological aspects of the disease.[1] Yet from a physical point of view, application of the planned dose in multiple fractions corresponds to a repeated experiment with uncertain outcome due to unknowns in the process such as range and setup uncertainties. The confidence intervals on the delivered dose distribution depend on the interplay of systematic errors (which are the same for every fraction) and random errors (which vary for different fractions). Automatically, this induces a dependence also on the number of chosen fractions.[2–5]

The common approach to compensate for uncertainties in photon therapy is to define a planning target volume (PTV) that extends the treatment fields beyond the clinical target volume. For particle therapy, this approach does not suffice, as the static dose cloud approximation[6] may fail due to the physical characteristics of particle beams, where variations in calculations of the water-equivalent path-length (WEPL) as well as daily patient-setup strongly influence the geometrical position of the Bragg-Peak inside the patient.[5,7,8] As a consequence intrinsically more robust dose delivery schemes, like single field uniform dose optimization (SFUD), may be applied.[9–11] Recent academic approaches, however, commonly employ explicit estimation of dose uncertainty in the form of worst cases or expectation value and standard deviation of dose. They are mostly based on dose scenario sampling,[12] followed by either margin adaptation[13] or application of robust or probabilistic treatment plan optimization methods.[14–17]

Computing a dose uncertainty metric for a treatment in F fractions, however, imposes additional complexity on the sampling methods. A single treatment sample comprises not only one systematic inter-fraction error scenario but F combinations of one systematic error with F random errors.[12,18] This increases the sampling run-time at least linearly with the number of fractions. To avoid the increased computational complexity emerging from this interplay, different sources of uncertainty have been, for example, considered separately either to be only systematic or random in nature.[19,20] Alternatively, polynomial chaos expansion has been suggested as a meta model to account for random and systematic uncertainties at the same time.[21]

However, when it comes to treatment plan optimization, sampling techniques or sur-

rogate dose models often become intractable since the dose distribution changes due to adaptations of the radiation fluences which means that the uncertainty metric needs to be recomputed. Consequently, existing methods use sparse sampling, e.g. considering only 10 scenarios to estimate mean and standard deviation of dose, during each iteration[17] and may exploit the assumption of infinite fractions to omit a complex, fractionation dependent variance computation while maintaining the induced "blurring" effect in the expectation value of dose.[4,15,22] Assuming an infinite number of fractions, however, is debatable in the context of radiation therapy. This holds especially for hypo-fractionated treatments using 5 fractions or less, which is regularly exercised in mixed-modality treatments with a particle boost.[23,24] Furthermore, working with the assumption of an infinite number of fractions during optimization may lead to highly inhomogeneous dose distributions[4,15] since the optimizer considers an infinite canceling out of random error contributions.

In previous work, we showed that uncertainty propagation with analytical probabilistic modeling (APM)[25,26] can overcome the aforementioned limitations through the definition of an completely analytic and integrable—in this case Gaussian—parameterization of the pencil-beam dose calculation algorithm. This enables the closed-form computation of the expectation value as well as the variance of a proton dose distribution considering range and setup errors. In particular it is possible to distinguish between random and systematic errors in the context of APM enabling probabilistic analysis and optimization of fractionated treatments at high accuracy of the uncertainty propagation itself.

In this paper, we further exploit the APM formalism to efficiently compute a linear model of the fractionation-dependent variance of dose subject to random and systematic components. This allows computing the variance of the dose distribution for all possible fraction numbers, i.e. the complete fractionation spectrum, for probabilistic analysis and optimization at the same time. We apply this method on three patient cases, and evaluate the conventional and probabilistic plans for different fractionation schemes based on the linear variance model. Results are compared against independent random Monte Carlo samples. Finally, this paper investigates the effects of the incorporation of explicit fractionation assumptions in probabilistic optimization. While this paper focuses on the application of APM, it also provides general information regarding treatment planning under explicit consideration of fractionation for sampling-based methods.

II. MATERIALS & METHODS

II.A. Analytical Probabilistic Modeling

The APM framework analytically maps range and setup errors to moments of the dose distribution.[25] To do so, APM assumes lateral, spatially factorized pencil-beam misplacements, i.e. setup errors, and uncertainty in the WEPL, i.e. range errors, and facilitates an accurate Gaussian parameterization of a conventional pencil-beam algorithm.[27] Previously, we demonstrated accuracy and computational efficiency of APM for fractionated treatments with respect to the underlying dose model.[26] An in-depth introduction to the principal APM framework can be found in Bangert, Hennig, Oelfke[25]; we provide a brief recapitulation below.

II.B. General Formulation

APM is based on the dose influence matrix concept describing an element d_i of the dose vector $\boldsymbol{d} \in \mathbb{R}^V$ for all V voxels by

$$d_i = \sum_j D_{ij} w_j \ . \tag{1}$$

w_j is an element of the vector $\boldsymbol{w} \in \mathbb{R}^B$ containing all B pencil-beam weights and $D \in \mathbb{R}^{V \times B}$ is the dose influence matrix with its elements D_{ij} containing the dose influence of pencil-beam j in voxel i at unit intensity.

In analogy to the nominal dose $\boldsymbol{d}$, we can perform a similar mapping for the expectation value of dose $\mathrm{E}[\boldsymbol{d}]$

$$\mathrm{E}[d_i] = \sum_j \mathrm{E}[D_{ij}]\, w_j = \sum_j \mathcal{D}_{ij} w_j \tag{2}$$

with the expected dose influence matrix $\mathcal{D} = \mathrm{E}[D]$.

Computing the covariance of dose $\Sigma^{\boldsymbol{d}}_{il} = \mathrm{Cov}[d_i, d_l]$ requires a fourth-order covariance influence tensor $\mathcal{V} \in \mathbb{R}^{V \times B \times V \times B}$ mapping the pencil-beam weights $\boldsymbol{w}$ to the covariance via the quadratic form

$$\mathrm{Cov}[d_i, d_l] = \sum_{jm} \mathrm{Cov}[D_{ij}, D_{lm}]\, w_j w_m = \sum_{jm} \mathcal{V}_{ijlm} w_j w_m \ . \tag{3}$$

Hence, a tensor element $\mathcal{V}_{ijlm}$ can be understood as the influence of a pair of covarying pencil beams j and m to the covariance of dose in voxels i and l.

Evaluating Eq. (2) and especially Eq. (3) is non-trivial; storing of $\mathcal{V}$ is infeasible. Here, we use APM as laid out in previous works[25,26] to compute $\mathcal{D}$ and $\mathcal{V}$. APM describes single elements $\mathcal{D}_{ij}$ and $\mathcal{V}_{ijlm}$ as a product over univariate and bivariate normal distributions, respectively, which enables their computation in closed-form (compare Eqs. (13-18) in Bangert, Hennig, Oelfke[25] and/or Appendix A in Wahl *et al.*[26]). With access to single elements of $\mathcal{D}$ and $\mathcal{V}$ the dose (co)variance can be computed on-the-fly without storage of $\mathcal{V}$.

II.C. Optimization

State-of-the-art treatment planning utilizes objectives or constraints, which can be defined as general function of dose.[28] However, probabilistic treatment planning, i.e. optimization of the expectation value $\mathrm{E}[\mathcal{F}]$ of an objective function $\mathcal{F}$,[17] is usually based on the penalized squared objective function[29]

$$\mathcal{F}(\boldsymbol{w}) = (\boldsymbol{d} - \boldsymbol{d}^*)^\top P (\boldsymbol{d} - \boldsymbol{d}^*) \tag{4}$$

where $P = \mathrm{diag}(p_1, \ldots, p_i, \ldots, p_V)$ is a diagonal matrix containing the optimization penalties for individual voxels i and $\boldsymbol{d^*}$ corresponds to the prescribed dose.

The expectation value is then given by

$$\mathrm{E}[\mathcal{F}(\boldsymbol{w})] = \underbrace{\mathrm{tr}(P\Sigma^{\boldsymbol{d}})}_{\sum_i p_i \sum_{jm} \mathcal{V}_{ijim} w_j w_m} + \underbrace{(\mathrm{E}[\boldsymbol{d}] - \boldsymbol{d}^*)^\top P (\mathrm{E}[\boldsymbol{d}] - \boldsymbol{d}^*)}_{\sum_i p_i \left(\sum_j \mathcal{D}_{ij} w_j - d_i^*\right)^2} . \tag{5}$$

Note that the trace operation only requires the variance, and therefore only the elements of $\mathcal{V}$ with $i = l$ for its evaluation.

Minimization of Eq. (5) would require an evaluation of the summarized variance influence in each iteration. To enable efficient optimization, we can use APM's capability of evaluating single elements of $\mathcal{V}$ to construct helper objects. Particularly, an integral variance influence matrix Ω^v

$$\Omega^v = \sum_{i \in v} p_i \mathcal{V}_{ijim} \tag{6}$$

can be constructed for every volume of interest (VOI) v. Since Ω^v is independent of the optimization variable $\boldsymbol{w}$, re-computation of elements of $\mathcal{V}$ during optimization is not required:

$$\mathrm{tr}(P\Sigma^{\boldsymbol{d}}) = \sum_v \boldsymbol{w}^\top \Omega^v \boldsymbol{w} \ . \tag{7}$$

The separation for volumes is performed because the penalty factor p_i is usually the same for all voxels i in a VOI, i.e. $p^v = p_i \ \forall i \in v$. Consequently p^v can be pulled out of the summation in Eq. (6) and no re-computation of Ω^v is required across multiple optimization runs with different p^v.

Within this work, we compare the outcome of optimizations with Eqs. (4) and (5). Optimization with Eq. (4) will be referenced to as *conventional optimization*, whereas optimization with Eq. (5) will be denoted as *probabilistic optimization*.

II.D. Separation of the covariance influence

For fractionation, an element of the covariance influence tensor $\mathcal{V}_{ijlm}$ needs to be decomposed to account for the different impact of random and systematic uncertainties on the dose covariance of a full treatment with F fractions. Over the course of a treatment, random errors are only correlated within a single fraction, i.e. they are realized independently in each fraction, while systematic errors realize once and are therefore correlated over the whole treatment. Therefore, $\mathcal{V}_{ijlm}$ separates into three parts:[25,26]

$$\mathcal{V}_{ijlm} = \frac{\widetilde{\mathcal{V}}^{\mathrm{corr}}_{ijlm} + (F-1)\widetilde{\mathcal{V}}^{\mathrm{uncorr}}_{ijlm}}{F} - \mathcal{D}_{ij}\mathcal{D}_{lm} \ . \tag{8}$$

$\widetilde{\mathcal{V}}^{\mathrm{corr}}_{ijlm}$ describes a single fraction, including the full correlation model for both systematic and random errors. $\widetilde{\mathcal{V}}^{\mathrm{uncorr}}_{ijlm}$ describes the remaining fractions, keeping the full correlation model only for systematic errors but treating random errors as completely uncorrelated. The last term subtracts the mixed expectation value of dose influence $\mathcal{D}_{ij}\mathcal{D}_{lm}$, since both previously described terms only describe the non-central moment contribution.

Equation (8) can be expanded to

$$\mathcal{V}_{ijlm} = \frac{1}{F} \cdot \left[\widetilde{\mathcal{V}}^{\mathrm{corr}}_{ijlm} - \widetilde{\mathcal{V}}^{\mathrm{uncorr}}_{ijlm}\right] + \left[\widetilde{\mathcal{V}}^{\mathrm{uncorr}}_{ijlm} - \mathcal{D}_{ij}\mathcal{D}_{lm}\right] \ . \tag{9}$$

Equation (9) shows that $\mathcal{V}_{ijlm}$ can be modeled as a linear combination of $\mathcal{V}^{\mathrm{rand}}_{ijlm} = \widetilde{\mathcal{V}}^{\mathrm{corr}}_{ijlm} - \widetilde{\mathcal{V}}^{\mathrm{uncorr}}_{ijlm}$ and $\mathcal{V}^{\mathrm{sys}}_{ijlm} = \widetilde{\mathcal{V}}^{\mathrm{uncorr}}_{ijlm} - \mathcal{D}_{ij}\mathcal{D}_{lm}$ as

$$\mathcal{V}_{ijlm} = \frac{1}{F} \cdot \mathcal{V}^{\mathrm{rand}}_{ijlm} + \mathcal{V}^{\mathrm{sys}}_{ijlm} \ . \tag{10}$$

Furthermore, the linear model in Eq. (10) also generalizes to derived quantities like the (co)variance in dose computed via Eq. (3)

$$\sigma_{\boldsymbol{d}}^2(F) = \frac{1}{F} \cdot \sigma_{\boldsymbol{d}}^{\mathrm{rand}\,2} + \sigma_{\boldsymbol{d}}^{\mathrm{sys}\,2} \tag{11}$$

or the helper matrix Ω described in Eq. (6)

$$\Omega^v(F) = \sum_{i \in v} p_i \left[\mathcal{V}_{ijlm}^{\mathrm{sys}} + \frac{\mathcal{V}_{ijlm}^{\mathrm{rand}}}{F} \right] = \Omega_{\mathrm{sys}}^v + \frac{\Omega_{\mathrm{rand}}^v}{F} \ . \tag{12}$$

Since all elements $\widetilde{\mathcal{V}}_{ijlm}^{\mathrm{corr}}$, $\widetilde{\mathcal{V}}_{ijlm}^{\mathrm{uncorr}}$ and $\mathcal{D}_{ij}\mathcal{D}_{lm}$ are available from APM, both the random and systematic components $\mathcal{V}_{ijlm}^{\mathrm{rand}}$ and $\mathcal{V}_{ijlm}^{\mathrm{sys}}$, as well as the random and systematic components of $\sigma_{\boldsymbol{d}}^2$ and Ω^v can be computed on-the-fly at minimum overhead. Note that the expectation value of dose is independent from the number of fractions, since it is in general invariant under different correlation assumptions by only depending on the sum of random and systematic variance in the input model.

Using $\Omega^v(F)$ in probabilistic optimization of the expected objective function in Eq. (5) induces dependence on the number of fractions F in the variance term (see Eq. (7)). This means that for a change in F Eq. (5) needs to be re-optimized, but since $\Omega^v(F)$ can be separated with Eq. (12), no-recomputation of the uncertainty mapping is needed between optimization runs.

Equations (10) to (12) apply equally to other methods capable of evaluating elements of $\mathcal{V}$ for the same correlation model of fractionation (random errors are uncorrelated for different fractions while systematic errors are perfectly correlated for different fractions). Equation (11) could be, for example, modeled by linear regression on the sample variance computed from samples of treatments with different fractionation schemes, yielding estimates for $\sigma_{\boldsymbol{d}}^{\mathrm{rand}\,2}$ and $\sigma_{\boldsymbol{d}}^{\mathrm{sys}\,2}$. Contrary to APM, however, sampling methods suffer from increased complexity under fractionation while at the same time inducing a statistical error that is anti-proportional to the square root of the number of samples.

II.E. Plan analysis

To investigate the capabilities of APM for uncertainty analysis of fractionated treatments, we analyze the variability of treatment plans generated by conventional and probabilistic

optimization under fractionation. Therefore we evaluate the output of APM, i.e. the standard deviation distributions and its separations, as well as reference computations based on sampling for both conventional and probabilistic plans. We use a spatially separated, multivariate uncertainty model; range as well as setup errors of pencil-beams belonging to the same beam direction are perfectly correlated, while beams from different directions are assumed to be statistically independent. All computations are performed for a prostate, a paraspinal and an intracranial case. The three cases have been chosen to represent different geometries and uncertainty assumptions: In the prostate case, the main treatment planning trade-off lies in lateral direction between the rectum and the target volume, which is irradiated with laterally opposed fields. In the paraspinal case the spinal cord lies in the center of the target volume. The intracranial case has a critical beam arrangement with the brainstem next to the distal edge of both beam directions. More information on the patients, assumed uncertainties and optimization parameters are listed in Table S-1 in the Supplementary Material.

The APM-based uncertainty analysis uses exemplary slices from the expected dose and standard deviation distributions, and standard deviation volume histograms (SDVHs),[4] which are constructed from the standard deviation distribution in analogy to dose-volume histograms (DVHs). To emphasize on the fractionation dependence, we will refer to plots displaying SDVHs for multiple fractions as *fractionated* SDVH (FSDVH).

For the sampling-based part of our uncertainty analysis, we apply random Monte Carlo sampling in the input space and compute the respective dose distribution. For all plans, 100 systematic scenarios are sampled with 30 random fractions each, totaling in 3000 computed dose scenarios per optimized plan. When different fractionation schemes are investigated for the same plan, dose accumulation for hypo-fractionation (i.e. $F = \{1, 2, 5, 10\}$) is performed on independent fraction subsets to omit autocorrelation between fraction samples. The resulting treatment dose scenarios are then used to compute percentile DVHs (PDVHs) as described in Gordon *et al.*[30], which, given a percentile q, plot the dose-volumes received with probability q versus dose.

III. RESULTS

III.A. Computation of the linear (co)variance model

Figure 1 displays results of APM variance calculation with fractionation separation for a prostate case.

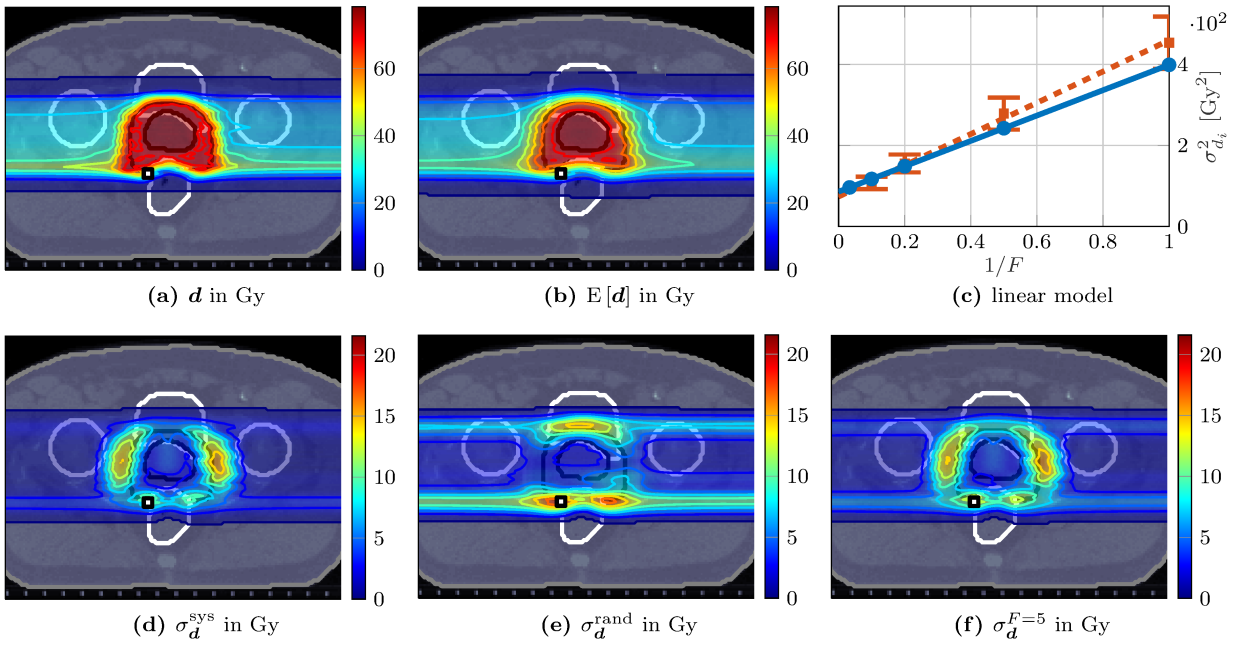

(a) $\boldsymbol{d}$ in Gy **(b)** E$[\boldsymbol{d}]$ in Gy **(c)** linear model

(d) $\sigma_{\boldsymbol{d}}^{\text{sys}}$ in Gy **(e)** $\sigma_{\boldsymbol{d}}^{\text{rand}}$ in Gy **(f)** $\sigma_{\boldsymbol{d}}^{F=5}$ in Gy

Fig. 1: Probabilistic analysis based on an exemplary axial slice of a prostate plan under fractionation. (a) shows the nominal dose, (b) its expectation value. (d) and (e) show the systematic and random components of the standard deviation computed by APM with (f) being the full standard deviation for 5 fractions. (c) illustrates the linear variance model (in the voxel with maximum variance at $F = 1$, indicated by a square marker in the distributions) by comparing the APM variance for F fractions (blue points) to the sample variance (orange squares, error bars correspond to $\pm 1\sigma$) and the respective linear models computed on-the-fly by APM (blue line) and based on the sample statistics (orange dashed line).

The obtained random and systematic components follow intuitive expectations; the systematic component $\sigma_{\boldsymbol{d}}^{\text{sys}}$ is dominated by high uncertainty at the distal and proximal tumor edges, which is induced by the dominating systematic range error and low influence of systematic setup errors (compare Table S-1). Similarly, the random component $\sigma_{\boldsymbol{d}}^{\text{rand}}$ is dominated by high uncertainty in lateral dose gradients induced by the larger random setup error.

For one voxel, we also visualize the linear model (Fig. 1c) for the complete fractionation spectrum of $[1, \infty)$ fractions, comparing it to the sample variance from 100 randomly chosen systematic scenarios with 30 random fractions each, from which we reconstructed fractionated treatments for 1, 2, 5 and 10 fractions without replacement of fraction samples to omit auto-correlations.

For the intracranial and paraspinal case the Supplementary Material contains a similar analysis in Figs. S-2 and S-3.

III.B. Evaluation of the full fractionation spectrum

With the components $\sigma_{\boldsymbol{d}}^{\text{sys}}$ and $\sigma_{\boldsymbol{d}}^{\text{rand}}$ available, the complete fractionation spectrum becomes accessible and the influence of the random component for different fraction numbers can be investigated. In Fig. 2 we show FSDVHs for the conventional plans of every case to visualize the impact of fractionation on dose uncertainty for entire volumes of interest.

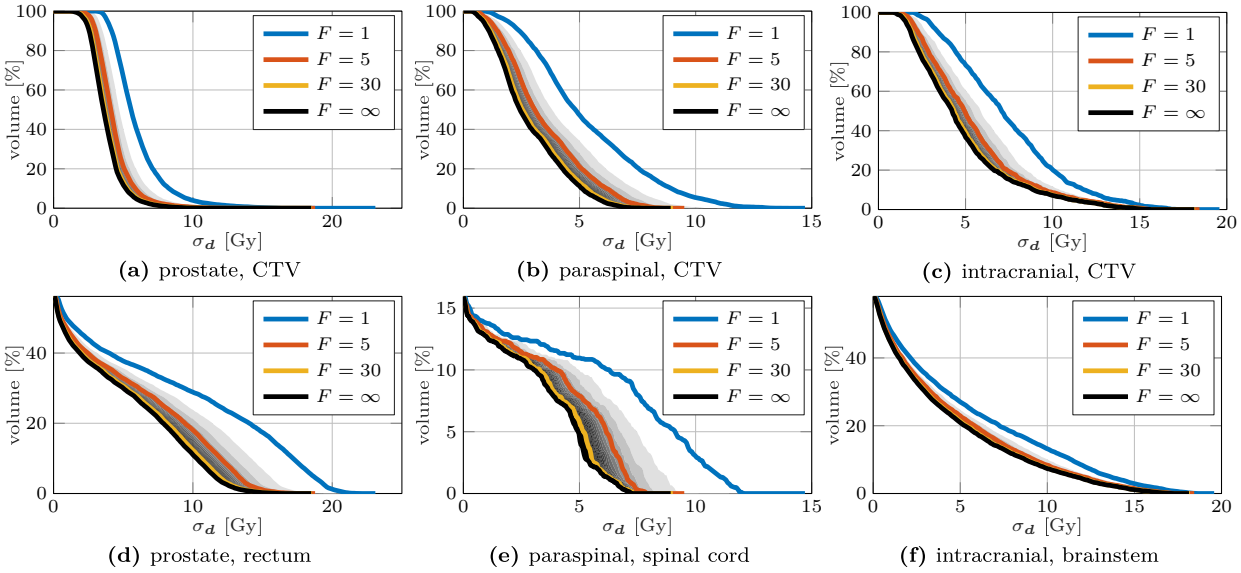

Fig. 2: FSDVHs for 1, 5, 30 and theoretically ∞ fractions of all cases for a target (top row) and OAR (bottom row), respectively. To illustrate the direct availabilty of the full fractionation spectrum by APM, each transition in the gray-shaded area corresponds to the SDVH of a treatment with one more fraction.

Figure 2 shows that the relative influence of random and systematic components may vary among structures and cases. For example, in case of the intracranial case, the uncertainty in the brainstem is dominated by systematic range uncertainties since it is located directly

next to the distal tumor edge with respect to both beams. Therefore uncertainty does not decrease as much by increasing the fraction number as in case of the rectum for the prostate case where random lateral setup uncertainty play a more important role. Observations for targets are more consistent for all three cases. This can be attributed to a more similar dose distribution, namely a homogeneous dose covering the entire structure with a surrounding gradient.

For all evaluated VOIs, we observe a rapid decrease towards the systematic limit with the fraction number, which is in line with the theoretical model of a F^{-1} dependence. While choosing 5 fractions over 1 fraction significantly decreases plan variability, a less significant decrease can be seen when choosing 30 over 5 fractions, with 30 fractions showing almost no difference in standard deviation compared to an infinite number of fractions. This behavior was also already observed in Perkó *et al.*[21] (more precisely in the supplementary materials), and suggests that for (non-hypofracionated) treatment optimized without uncertainty considerations, increasing the fractionation number for the sake of mitigating random uncertainties can be expected to have minimal to neglectible benefit.

III.C. Probabilistic optimization considering different fractionation schemes

Using the separated Ω^v-matrices from Eq. (12), probabilistic treatment plans could be optimized for different fractionation schemes without re-computing variance information. The resulting treatment plans are compared against treatment plans facilitating conventional optimization not making any fractionation assumption. A sampling-based evaluation of the prostate case considering fractionation is shown in Figure 3. The remaining intracranial and paraspinal cases can be found in the Supplementary Material as Figs. S-4 and S-5. For both the conventional and probabilistically optimized plans, significant reduction in plan variability can be observed when going from 1 to 5 and 30 fractions. However, the difference between 5 and 30 fractions is less significant, confirming the rapidly decreasing influence of the random error component with the number of fractions already shown in the FSDVHs in Fig. 2. Probabilistic optimization yields more robust target coverage than conventional optimization. This can be seen by the PDVHs being closer to the nominal DVH for all fractionation schemes.

Figure 4 directly compares conventional to probabilistic optimization under fractionation

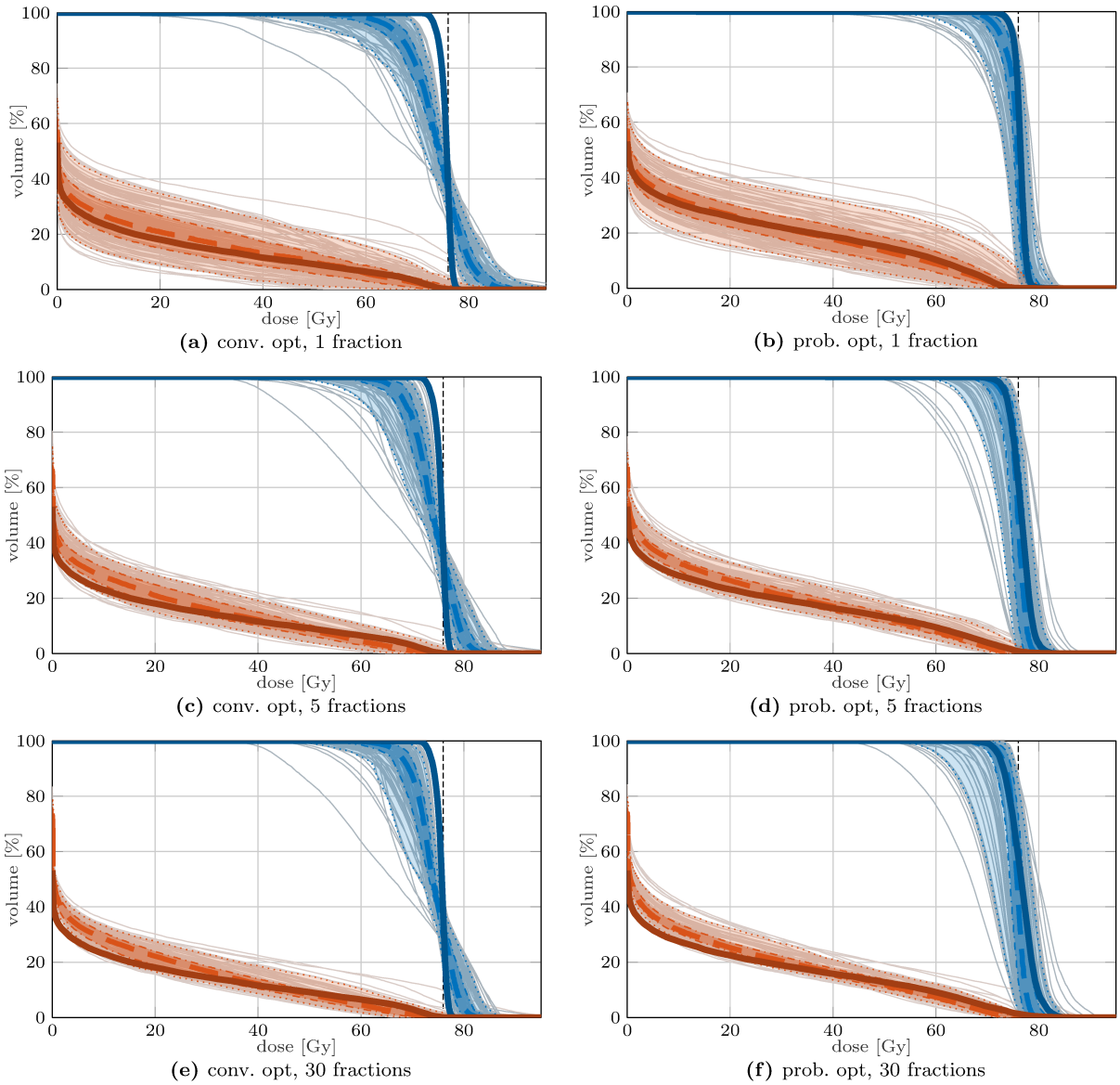

(a) conv. opt, 1 fraction

(b) prob. opt, 1 fraction

(c) conv. opt, 5 fractions

(d) prob. opt, 5 fractions

(e) conv. opt, 30 fractions

(f) prob. opt, 30 fractions

Fig. 3: Sampling based evaluation of a conventionally optimized prostate plan for several fractionation schemes (left) compared to probabilistic plans optimized with fractionation information (right). Blue lines refer to the target boost, orange lines to the rectum. Solid lines are nominal DVHs, dashed lines are the median DVH (or 50 % PDVH), while the shaded areas (enclosed by the thin dotted and the dash-dotted lines) refer to the 5 % to 95 % PDVH and 25 % to 75 % PDVH quantiles respectively.

for all cases. We show the median DVHs (50 % PDVHs) for targets and organs-at-risk (OARs).

The impact of probabilistic optimization depending on the fractionation scheme is patient-specific. In general, probabilistic optimization shifts the targets' median DVHs to higher

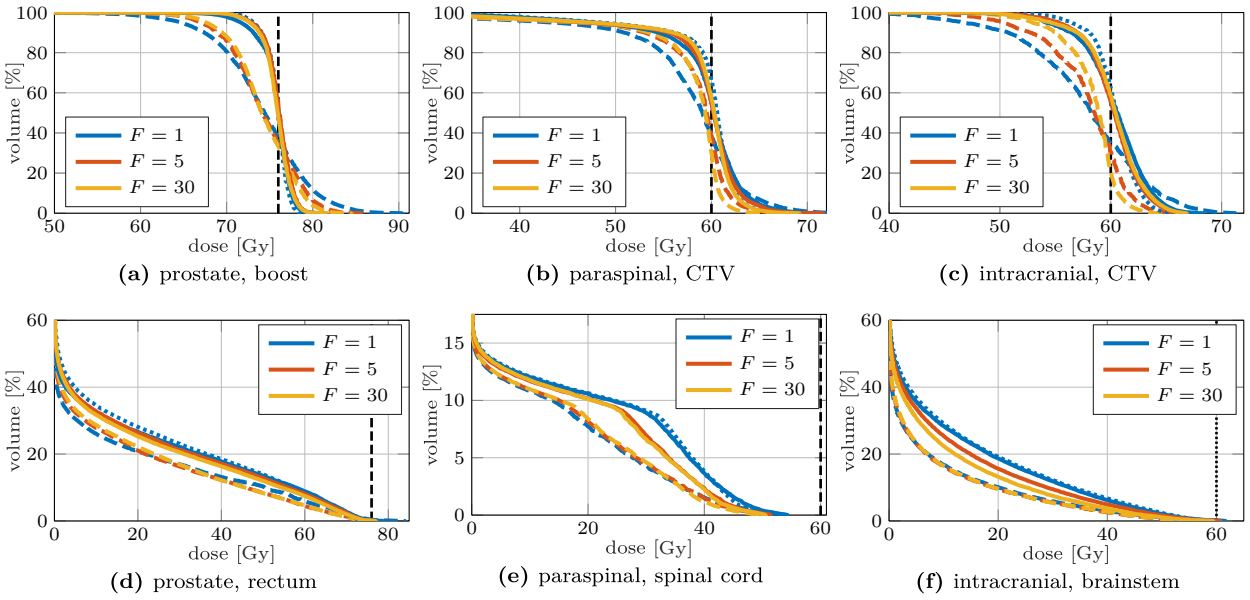

Fig. 4: Median DVHs (50 % PDVHs) for all cases after conventional optimization (dashed) and probabilistic optimization (solid) for the fractionation schemes $F = \{1, 5, 30\}$. For each case, a target (top row) and an OAR (bottom row) is presented. The dotted blue lines represent plans optimized for a single fraction, but applied in 30 fractions. The vertical dashed black line indicates the prescribed dose for the respective target.

doses, increasing the probability of target coverage. This can be seen especially in Figs. 4a and 4c for the prostate and intracranial case while it is not so pronounced in the paraspinal case (Fig. 4b). Across different fractionation schemes, the median DVHs after probabilistic optimization show only marginal differences (with the curves lying on top of each other). For the para-spinal case, however, we see a strong effect in the OAR, i.e. the spinal cord (Fig. 4e), where the median dose-volume is increased by probabilistic optimization. While the median DVHs for $F = 5$ and $F = 30$ fractions are almost identical, a prominent shift to higher dose-volumes can be seen for $F = 1$. For the other two cases, the fraction dependence is evident yet less present. For the rectum (Fig. 4d) differences are in general much smaller, also when comparing conventional to probabilistic optimization. Consequently, probabilistic optimization adapts to the increasing number of fractions and improves the trade-off between target coverage and OAR sparing.

III.C.1. Generalization of probabilistic plans among fractionation schemes

Figure 4 additionally shows the median DVHs of a treatment plan optimized probabilistically for a single fraction and applied in 30 fractions. This enables a comparison between (1) using and (2) neglecting explicit fractionation information during optimization. For the target volumes, there is only a very minor difference. Both treatment plans that were optimized probabilistically for one fraction to be subsequently applied in 30 fractions and treatment plans that were optimized probabilistically for 30 fraction to be subsequently applied in 30 fractions result in approximately the same median DVH. For the OARs, however, we see that optimization explicitly considering 30 fractions results in a better sparing than optimization considering a single fraction. This behavior is especially pronounced in the spinal cord (Fig. 4e).

To substantiate these results, box plots for dose quality metrics were generated from the sampled plans in Fig. 5. For the targets, $D^{95\,\%}$, i.e. the dose received by at least 95 % of the volume, is shown. For the OARs, the metrics are chosen based on Marks *et al.*[31]; $D^{5\,\%}$ is used as a maximum dose indicator for spinal cord and brainstem, while the rectum is evaluated based on $V^{50\,\mathrm{Gy}}$, i.e. the volume covered by at least a dose of 50 Gy.

As already shown in Fig. 4, expected target coverage increases with probabilistic optimization, as well as OAR dose, i.e. OAR sparing is traded against robustness. When neglecting the fractionation number in the probabilistic optimization, Fig. 5 illustrates that for the OARs, the median, the expected value as well as the entire probability mass of the dose quality indicators is unecessarily high compared to plans directly optimized for the respective number of fractions. This holds for 5 fractions as well as 30 fractions. For the targets, this effect is also visible, but less pronounced than in the OARs.

Figure 6 further illustrates above observations with the FSDVHs for cross-application of probabilistically optimized treatment plans in a different number of fractions.

For the target volumes of all cases (Figs. 6a to 6c), the probabilistic treatment plans optimized for $F = 1$ yield consistently lower dose uncertainty for application in 5 or 30 fractions than the treatment plans explicitly optimized for the respective number of fractions. For OARs (Figs. 6d to 6f), this behavior persists in the high dose standard deviation regions yet at more variation among cases. It can be explained through the higher contribution of the variance term $\mathrm{tr}(P\Sigma^{\boldsymbol{d}})$ within $\mathrm{E}[\mathcal{F}]$ with decreasing fraction number, leading to an

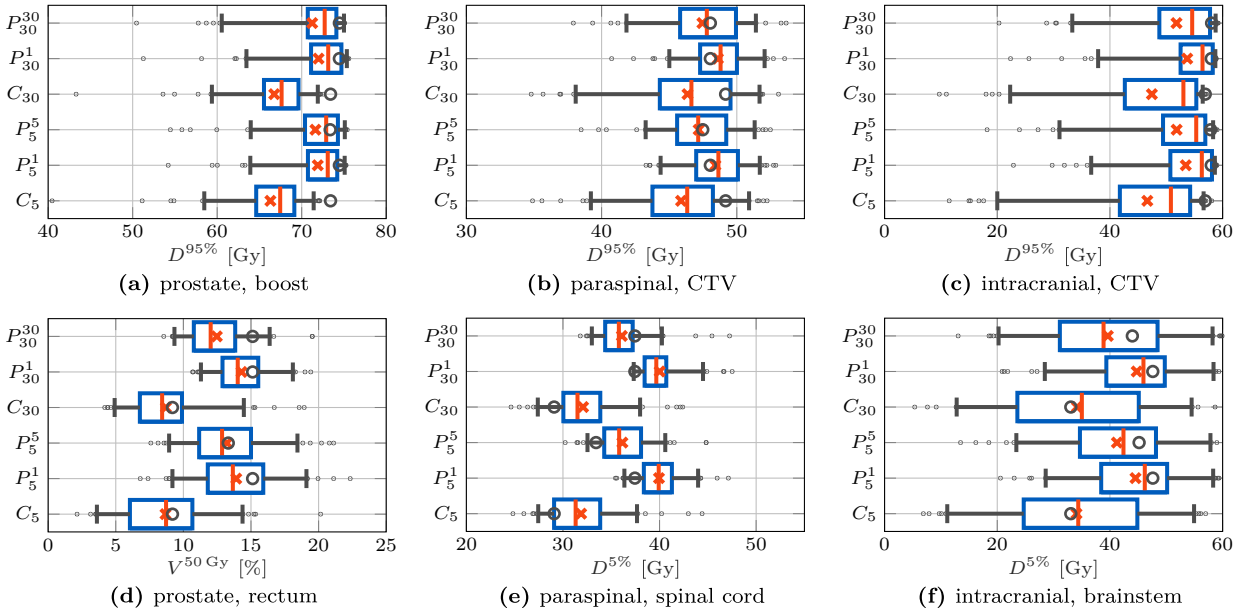

(a) prostate, boost **(b)** paraspinal, CTV **(c)** intracranial, CTV

(d) prostate, rectum **(e)** paraspinal, spinal cord **(f)** intracranial, brainstem

Fig. 5: Box plots for dose quality metrics comparing samples from conventional plans C_F, where F is the number of fractions they are applied in, and probabilistically optimized plans P_F^A, where A is the number of fractions used for optimization. Analogous to Fig. 3, the box and the whiskers enclose the 25 % to 75 % and 5 % to 95 % quantiles, respectively. The vertical markers indicate the median, crosses the mean value, and the circle the respective value computed from the nominal dose distribution.

increased focus on reducing plan variability instead of carefully shaping the expected dose to prescription during optimization. For 30 fractions, for example, a more heterogeneous nominal dose distribution might be tolerated, since it is expected to smooth out due to random fraction scenario realizations. This effect will be further discussed in the section below.

III.C.2. Beam modulation depending on number of fractions

Probabilistic optimization under the assumption of infinite fractions may lead to heterogeneous nominal dose distributions, since a homogeneous distribution of the expectation value of dose may be achieved by optimizing for perfectly destructive interference of infinite random scenarios.[4,15] As APM explicitly incorporates finite number of fractions, the optimized fluences change with fractionation scheme, as can be seen in Fig. 7 for the prostate case. While for conventional optimization the beam shows the most distinct modulation,

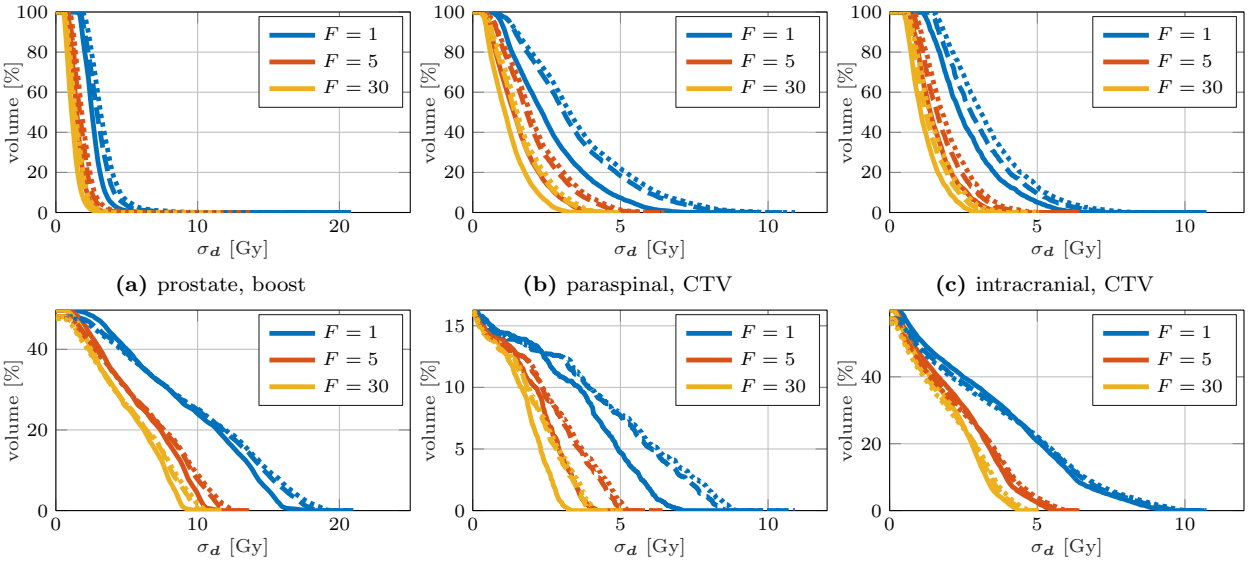

(a) prostate, boost **(b)** paraspinal, CTV **(c)** intracranial, CTV

(d) prostate, rectum **(e)** paraspinal, spinal cord **(f)** intracranial, brainstem

Fig. 6: FSDVH comparison for probabilistically optimized plans when applied to other fractionation schemes for a target and OAR of all cases. Color represents the applied fractionation schemes, i.e. all lines of the same color are applied in the same number of fractions, whereas line style represents the initially chosen fraction number for optimization: solid lines correspond to probabilistic plans optimized for $F = 1$, dashed lines $F = 5$ and dotted lines $F = 30$.

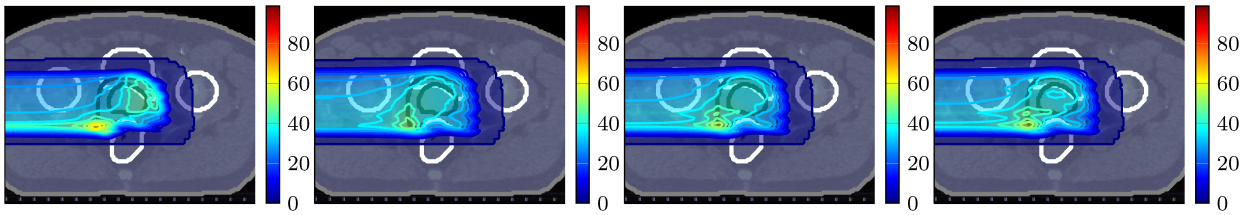

(a) conv. opt. **(b)** prob. opt., $F = 1$ **(c)** prob. opt., $F = 5$ **(d)** prob. opt., $F = 30$

Fig. 7: Dose (in Gy) of the 270° prostate beam after conventional (a) and probabilistic optimization for several fractionation schemes (b-d).

probabilistic optimization creates much smoother dose distributions for individual beams. Low fraction numbers lead to the smoothest dose distribution while an increasing fraction count F allows for additional modulation as canceling out of random error contributions during the treatment becomes more probable.

335 This effect is substantiated in the DVHs in Figs. 3b, 3d and 3f, where probabilistic optimization for $F = 1$ enforces a steep decrease of the nominal DVH equivalent to a more homogeneous dose distribution in the target, whereas optimization for $F > 1$ shows less

steep DVHs and therefore more heterogeneous dose distributions. Yet for the $F = 1$ case, with no possibility of inter-fractional error cancellation, the median DVH is more flat than the nominal dose-volume histogram while it is more steep than the nominal DVH in the case of 30 fractions, where the canceling out of random errors can be expected.

IV. DISCUSSION

With the APM framework, we constructed an efficient dose variance computation pipeline that explicitly models the dependence of dosimetric uncertainties on the number of treatment fractions. We showed that dose variance calculations can generally be modeled with a linear relationship whose parameters can be determined from first principles with APM. The linear model was used to perform dose uncertainty analysis for all possible fraction numbers $F \in [1, \infty)$ for three different patient cases. Furthermore, the linear variance calculation model was incorporated into probabilistic optimization which enabled a study of the interdependence of the number of fractions and dosimetric treatment plan quality/robustness within numerical treatment plan optimization.

The linear relationship for variance computation follows directly from the underlying standard definition of systematic and random errors in the input parameters, namely that systematic errors are perfectly correlated (i.e. they are exactly the same) for all treatment fractions and random errors are completely uncorrelated.[12,18–21] In principle, the linear variance computation model can be constructed with any uncertainty propagation method that is able to compute the dose uncertainty for at least two fractionation schemes. However, a sampling-based construction is inevitably sensitive to sampling uncertainties (Fig. 1c). A construction based on APM, in contrast, allows for the separate computation of the full covariance influence. Thus, the whole model can be constructed on-the-fly while additionally generalizing to optimization. This incidental incorporation of the fraction number as parameter into the objective function, weighting random against systematic variance influence, could enable the incorporation of intuitive fractionation objectives in the future. Furthermore, no statistical uncertainties are induced by APM; the model is intrinsically guaranteed to be physically meaningful while simple linear regression on uncertain, fractionation-dependent sampling variances might lead to negative systematic or random variance components. Hence we only presented comparisons of APM to regression in single

voxels in Figs. 1c, S-2c and S-3c. While these analyses on the respective maximum variance voxel may illustrate possible variations, they should only be judged qualitatively due to low sample numbers and since they only represent local voxel information; where a single voxel might apparantly exhibit biased behavior, the neighboring voxel may show nearly perfect agreement. A detailed analysis of the accuracy (and possible bias) of the APM method based on full distributions can be found in Wahl *et al.*[26]. Even though the used uncertainty model in the input space is based on common assumptions found in literature, i.e. perfectly correlated shifts and inter-fractional separation in random and systematic error components, it still excludes a variety of effects such as complex motion patterns and deformation. Despite these shortcomings, including fractionation was found to have a non-trivial effect on probabilistic optimization. The definition of more sophisticated uncertainty models, e.g. based on daily image guidance, is to be addressed for many methods using robust or probabilistic optimization techniques. Further, in a clinical environment additional efforts and protocols might interfere with the strict application of a physical model. While, for example, fractionation dependent prescribed dose could be easily incorporated in the presented methodology, it would be non-trivial to seamlessly consider fractionation dependent clinical uncertainty mitigation efforts without re-computations. Yet, tools like presented in this work, may help to assess the necessity or success of these clinical mitigation efforts in such environments.

The three patient cases were evaluated for different fraction numbers in comparison to random sampling[12,18] of treatment plans that were established using both conventional and probabilistic optimization. Since the comparably low number of 100 treatment samples prohibit a statistically meaningful analysis of dose coverage criteria or extreme dose values, we laid focus on the median outcome of all sampled treatments. Modeling fractionation effects in APM includes the trade-off between nominal dose and robustness in optimization. This functionality is challenging or impossible to produce in other frameworks. While for photon therapy, studies already evaluated the impact of fractionation in probabilistic or robust optimization,[4,22] for proton therapy the exact incorporation of the number of fractions is avoided or enabled by further simplifications of the uncertainty model. For example, Lowe *et al.*[19,20] strictly separate setup errors to be random and range errors to be systematic. Unkelbach *et al.*[17] do not consider random errors at all. Fredriksson[15] assumes uncertainty on the probability distribution of the random errors itself to avoid heterogeneous dose distributions when assuming infinite fractions.

The excessive random scenario sampling used in this study, with run-times of several days, is not feasible in a clinical environment, especially for treatment plan optimization. For the latter, APM may be more applicable despite existing limitations of the underlying pencil-beam algorithm. Furthermore, expected value optimization as applied in this work is a non-conservative method.[15] While it yields a more robust treatment on average, it does not guarantee robustness against worst cases. Additionally, the performance of optimizing the expected value is limited by the objective function it is based on. To enable generalization to worst case optimization methods and state-of-the-art objective functions, further development with regard to constrained probabilistic planning similar to conditional value at risk optimization[15,32,33] is desirable. The necessary non-trivial generalizations to expectation and variance of clinical objectives are part of ongoing research to reveal the full potential—and limitations—of the APM method to enable more intuitive probabilistic treatment planning.

V. CONCLUSION

Based on analytical probabilistic modeling, we devised a linear fractionation model considering the non-trivial interplay of random and systematic components of range and setup errors for fractionated proton treatments. In the analytical probabilistic modeling framework, the model enables efficient dose variance computation as well as probabilistic treatment plan optimization under fractionation.

We used the fractionation-dependent variance model to expose the trade-off between number of fractions, nominal dose, and treatment plan robustness for three different patient cases. Considering the number of fractions during treatment plan optimization we could provide evidence that the explicit incorporation of fractionation may allow for the exploitation of an improved trade-off between target coverage and organ-at-risk sparing in intensity-modulated proton therapy.

ACKNOWLEDGMENTS

The authors acknowledge financial support from the German Research Foundation, Grant No. BA 2279/3-1.

DISCLOSURE OF CONFLICTS OF INTEREST

The authors have no relevant conflicts of interest to disclose.

REFERENCES

[1]Joiner M, van der Kogel AJ, eds. *Basic clinical radiobiology*. 4th ed. London: Hodder Arnold; 2009.

[2]van Herk M, Witte M, van der Geer J, Schneider C, Lebesque JV. Biologic and physical fractionation effects of random geometric errors. *Int J Radiat Oncol Biol Phys*. 2003;57(5):1460–1471.

[3]Chu M, Zinchenko Y, Henderson SG, Sharpe MB. Robust optimization for intensity modulated radiation therapy treatment planning under uncertainty. *Phys Med Biol*. 2005;50(23):5463–5477.

[4]Unkelbach J, Oelfke U. Inclusion of organ movements in IMRT treatment planning via inverse planning based on probability distributions. *Phys Med Biol*. 2004;49(17):4005–4029.

[5]Lomax AJ. Intensity modulated proton therapy and its sensitivity to treatment uncertainties 2: the potential effects of inter-fraction and inter-field motions. *Phys Med Biol*. 2008;53(4):1043–1056.

[6]Bortfeld T, Jiang SB, Rietzel E. Effects of motion on the total dose distribution. *Semin Radiat Oncol*. 2004;14(1):41–51.

[7]Lomax AJ. Intensity modulated proton therapy and its sensitivity to treatment uncertainties 1: the potential effects of calculational uncertainties. *Phys Med Biol*. 2008;53(4):1027–1042.

[8]Albertini F, Hug EB, Lomax AJ. Is it necessary to plan with safety margins for actively scanned proton therapy? *Phys Med Biol*. 2011;56(14):4399–4413.

[9]Albertini F, Hug EB, Lomax AJ. The influence of the optimization starting conditions on the robustness of intensity-modulated proton therapy plans. *Phys Med Biol*. 2010;55(10):2863–2878.

[10]Liu W, Li Y, Li X, Cao W, Zhang X. Influence of robust optimization in intensity-modulated proton therapy with different dose delivery techniques. *Med Phys*. 2012;39(6):3089–3101.

[11]Zhu XR, Poenisch F, Li H, et al. A single-field integrated boost treatment planning technique for spot scanning proton therapy. *Radiat Oncol*. 2014;9:202.

[12]Park PC, Cheung JP, Zhu XR, et al. Statistical assessment of proton treatment plans under setup and range uncertainties. *Int J Radiat Oncol Biol Phys*. 2013;86(5):1007–1013.

[13]Knopf AC, Boye D, Lomax A, Mori S. Adequate margin definition for scanned particle therapy in the incidence of intrafractional motion. *Phys Med Biol*. 2013;58(17):6079–6094.

[14]Fredriksson A, Forsgren A, Hårdemark B. Minimax optimization for handling range and setup uncertainties in proton therapy. *Med Phys*. 2011;38(3):1672–1684.

[15]Fredriksson A. A characterization of robust radiation therapy treatment planning methods—from expected value to worst case optimization. *Med Phys*. 2012;39(8):5169–5181.

[16]Liu W, Zhang X, Li Y, Mohan R. Robust optimization of intensity modulated proton therapy. *Med Phys*. 2012;39(2):1079–1091.

[17]Unkelbach J, Bortfeld T, Martin BC, Soukup M. Reducing the sensitivity of IMPT treatment plans to setup errors and range uncertainties via probabilistic treatment planning. *Med Phys*. 2009;36(2009):149–163.

[18]Kraan AC, van de Water S, Teguh DN et al. Dose uncertainties in IMPT for oropharyngeal cancer in the presence of anatomical, range, and setup errors. *Int J Radiat Oncol Biol Phys*. 2013;87(5):888–896.

[19]Lowe M, Albertini F, Aitkenhead A, Lomax AJ, MacKay RI. Incorporating the effect of fractionation in the evaluation of proton plan robustness to setup errors. *Phys Med Biol*. 2016;61(1):413–429.

[20]Lowe M, Aitkenhead A, Albertini F, Lomax AJ, MacKay RI. A robust optimisation approach accounting for the effect of fractionation on setup uncertainties. *Phys Med Biol*. 2017;62(1):8178–8196.

[21]Perkó Z, van der Voort SR, van de Water S et al. Fast and accurate sensitivity analysis of IMPT treatment plans using Polynomial Chaos Expansion. *Phys Med Biol*. 2016;61(12):4646–4664.

[22]Chan TCY, Bortfeld T, Tsitsiklis JN. A robust approach to IMRT optimization. *Phys Med Biol*. 2006;51(10):2567–2583.

[23]Schulz-Ertner D, Tsujii H. Particle Radiation Therapy Using Proton and Heavier Ion Beams. *J Clin Oncol*. 2007;25(8):953–964.

[24]Combs SE, Kessel KA, Herfarth K et al. Treatment of pediatric patients and young adults with particle therapy at the Heidelberg Ion Therapy Center (HIT): establishment of workflow and initial clinical data. *Radiat Oncol*. 2012;7(1):170.

[25]Bangert M, Hennig P, Oelfke U. Analytical probabilistic modeling for radiation therapy treatment planning. *Phys Med Biol*. 2013;58(16):5401–5419.

[26]Wahl N, Hennig P, Wieser HP, Bangert M. Efficiency of analytical and sampling-based uncertainty propagation in intensity-modulated proton therapy. *Phys Med Biol*. 2017;62(14):5790–5807.

[27]Schaffner B, Pedroni E, Lomax A. Dose calculation models for proton treatment planning using a dynamic beam delivery system: an attempt to include density heterogeneity effects in the analytical dose calculation. *Phys Med Biol*. 1999;44(1):27–41.

[28]Wu Q, Mohan R. Algorithms and functionality of an intensity modulated radiotherapy optimization system. *Med Phys*. 2000;27(4):701–711.

[29]Oelfke U, Bortfeld T. Inverse planning for photon and proton beams. *Med Dosim*. 2001;26(2):113–124.

[30]Gordon JJ, Sayah N, Weiss E, Siebers JV. Coverage optimized planning: probabilistic treatment planning based on dose coverage histogram criteria. *Med Phys*. 2010;37(2):550–563.

[31]Marks LB, Yorke ED, Jackson A et al. The Use of Normal Tissue Complication Probability (NTCP) Models in the Clinic. *Int J Radiat Oncol Biol Phys*. 2010;76(3 Suppl):10–19.

[32]Romeijn HE, Ahuja RK, Dempsey JF, Kumar A, Li JG. A novel linear programming approach to fluence map optimization for intensity modulated radiation therapy treatment planning. *Phys Med Biol*. 2003;48(21):3521–3542.

[33]Rockafellar RT, Uryasev S. Optimization of conditional value-at-risk. *J Risk*. 1997;2:21–41.

FIGURE CAPTIONS

Fig. 1: Probabilistic analysis based on an exemplary axial slice of a prostate plan under fractionation. (a) shows the nominal dose, (b) its expectation value. (d) and (e) show the systematic and random components of the standard deviation computed by APM with (f) being the full standard deviation for 5 fractions. (c) illustrates the linear variance model (in the voxel with maximum variance at $F = 1$, indicated by a square marker in the distributions) by comparing the APM variance for F fractions (blue points) to the sample variance (orange squares, error bars correspond to $\pm 1\sigma$) and the respective linear models computed on-the-fly by APM (blue line) and based on the sample statistics (orange dashed line).

Fig. 2: FSDVHs for 1, 5, 30 and theoretically ∞ fractions of all cases for a target (top row) and OAR (bottom row), respectively. To illustrate the direct availabilty of the full fractionation spectrum by APM, each transition in the gray-shaded area corresponds to the SDVH of a treatment with one more fraction.

Fig. 3: Sampling based evaluation of a conventionally optimized prostate plan for several fractionation schemes (left) compared to probabilistic plans optimized with fractionation information (right). Blue lines refer to the target boost, orange lines to the rectum. Solid lines are nominal DVHs, dashed lines are the median DVH (or 50 % PDVH), while the shaded areas (enclosed by the thin dotted and the dash-dotted lines) refer to the 5 % to 95 % PDVH and 25 % to 75 % PDVH quantiles respectively.

Fig. 4: Median DVHs (50 % PDVHs) for all cases after conventional optimization (dashed) and probabilistic optimization (solid) for the fractionation schemes $F = \{1, 5, 30\}$. For each case, a target (top row) and an OAR (bottom row) is presented. The dotted blue lines represent plans optimized for a single fraction, but applied in 30 fractions. The vertical dashed black line indicates the prescribed dose for the respective target.

Fig. 5: Box plots for dose quality metrics comparing samples from conventional plans C_F, where F is the number of fractions they are applied in, and probabilistically optimized plans P_F^A, where A is the number of fractions used for optimization. Analogous to Fig. 3, the box and the whiskers enclose the 25 % to 75 % and 5 % to 95 % quantiles, respectively. The vertical markers indicate the median, crosses the mean value, and the circle the respective value computed from the nominal dose distribution.

Fig. 6: FSDVH comparison for probabilistically optimized plans when applied to other fractionation schemes for a target and OAR of all cases. Color represents the applied fractionation schemes, i.e. all lines of the same color are applied in the same number of fractions, whereas line style represents the initially chosen fraction number for optimization: solid lines correspond to probabilistic plans optimized for $F = 1$, dashed lines $F = 5$ and dotted lines $F = 30$.

Fig. 7: Dose (in Gy) of the 270° prostate beam after conventional (a) and probabilistic optimization for several fractionation schemes (b-d).